LES of MHD turbulent channel flows with a local SGS model based on coherent structures

By H. Kobayashi†

1. Motivation and objectives

An understanding of magnetohydrodynamic (MHD) turbulent flows is important to the control of liquid metal pumps, of MHD power generators, and of liquid metal heat exchangers in nuclear fusion reactors. Experiments and numerical simulations have been carried out to reveal the behavior of turbulence in a channel under the influence of a magnetic field.

For MHD turbulent channel flows under a uniform and strong magnetic field, it is well-known that laminarization arises in experiments (Brouillette & Lykoudis 1967; Reed & Lykoudis 1978). Note that each experiment is carried out in a rectangular cross-section duct of 5:1 or 5.8:1 aspect ratio with insulated walls. The Lorentz force acts against a streamwise flow. A skin friction coefficient C_f is generally plotted as a function of $Hr = Ha/Re \times 10^4$, where Ha is the Hartmann number and Re is the Reynolds number. The Hartmann number increases in proportion to the strength of the magnetic field. As the Hartmann number increases under the constant Reynolds number, the skin friction coefficient approaches a laminar line (i.e. a "two-dimensional" laminar solution).

In MHD turbulent channel flows, Shimomura (1991) performed large-eddy simulation (LES) with a calibrated model parameter against the experimental data of Brouillette & Lykoudis (1967), while Lee & Choi (2001) carried out direct numerical simulation (DNS) at low Reynolds number.

Knaepen & Moin (2004) have carried out LES using the dynamic Smagorinsky model (DSM) (Germano *et al.* 1991) with a least-squares procedure proposed by Lilly (1992) for the decaying homogeneous isotropic turbulence under the influence of an applied external magnetic field at low magnetic Reynolds number. From their results, in comparison with DNS for the same flow, it was shown that the LES with the DSM performs significantly better than the conventional Smagorinsky (1963) model (SM), because the Smagorinsky constant automatically decreases as the external magnetic field increases. Thus, the DSM has the potential to reproduce the transition from a turbulent MHD flow to a laminarized MHD flow without a special treatment for the magnetic field.

Recently, Kobayashi (2005) proposed local subgrid-scale (SGS) models based on coherent structures (CS) and showed the same performance as the DSM for homogeneous isotropic turbulences and for turbulent channel flows with and without rotation. The model is called the coherent-structure Smagorinsky model (CSM). This model does not need to average or clip the model parameter, to use an explicit wall-damping function, or to change the model constant. Therefore, like the DSM, this model has the potential to capture the transition without a special treatment for the magnetic field. In particular, the local calculation of the model parameter has the potential to represent the

† Permanent address: Keio University, Japan

fluctuations in the shear stress better than does the averaged determination of the model parameter in the DSM.

In the present study, the prediction of the transition from a turbulent MHD flow to a laminarized MHD flow is examined in a plane channel at a low magnetic Reynolds number with a uniform magnetic field perpendicular to insulated walls, using the CSM, the DSM, and the SM.

2. Governing equations and numerical methods

2.1. *Governing equations for grid-scale fields*

The system of governing equations for incompressible MHD flows is composed of the continuity equation, Navier-Stokes equations with the Lorentz force, the generalized Ohm's law, and Maxwell equations at low magnetic Reynolds number (Shimomura 1991),

$$\boldsymbol{\nabla}\cdot\mathbf{u} = 0, \tag{2.1}$$

$$\frac{\partial \mathbf{u}}{\partial t} + \mathbf{u}\cdot\boldsymbol{\nabla}\mathbf{u} = -\boldsymbol{\nabla}p + \nu\boldsymbol{\nabla}^2\mathbf{u} + \frac{1}{\rho}\mathbf{j}\times\mathbf{B}, \tag{2.2}$$

$$\mathbf{j} = \sigma(\mathbf{E} + \mathbf{u}\times\mathbf{B}), \tag{2.3}$$

$$\boldsymbol{\nabla}\cdot\mathbf{j} = 0, \tag{2.4}$$

$$\boldsymbol{\nabla}\times\mathbf{E} = \mathbf{0}, \tag{2.5}$$

where $\mathbf{u}$ is the velocity, p the pressure divided by the density, ν the kinematic viscosity, ρ the density, $\mathbf{j}$ the current density, $\mathbf{B}$ the magnetic field, σ the electrical conductivity, and $\mathbf{E}$ the electric field. At low magnetic Reynolds number, the induced magnetic field is negligible in comparison with a steady and uniform magnetic field $\mathbf{B}_0$ (Schumann 1976), so that the magnetic field in the present study is given by

$$\mathbf{B}(\mathbf{x}, t) = \mathbf{B}_0. \tag{2.6}$$

The electric field is described with the electric potential ϕ as

$$\mathbf{E} = -\boldsymbol{\nabla}\phi, \tag{2.7}$$

and from (2.3) and (2.4) the electric potential satisfies the following Poisson equation:

$$\boldsymbol{\nabla}^2\phi = \boldsymbol{\nabla}\cdot(\mathbf{u}\times\mathbf{B}_0) = \mathbf{B}_0\cdot\boldsymbol{\omega}, \tag{2.8}$$

where $\boldsymbol{\omega}$ denotes the vorticity, $\boldsymbol{\omega} = \boldsymbol{\nabla}\times\mathbf{u}$.

After a spatial filtering operation of the above equations, the governing equations for the grid-scale (GS) are given by

$$\boldsymbol{\nabla}\cdot\overline{\mathbf{u}} = 0, \tag{2.9}$$

$$\frac{\partial \overline{u}_i}{\partial t} + \overline{u}_j\frac{\partial \overline{u}_i}{\partial x_j} = -\frac{\partial \overline{p}}{\partial x_i} + \nu\boldsymbol{\nabla}^2\overline{u}_i - \frac{\partial \tau^a_{ij}}{\partial x_j} + \frac{\sigma}{\rho}[(-\boldsymbol{\nabla}\overline{\phi} + \overline{\mathbf{u}}\times\mathbf{B}_0)\times\mathbf{B}_0]_i, \tag{2.10}$$

$$\boldsymbol{\nabla}^2\overline{\phi} = \boldsymbol{\nabla}\cdot(\overline{\mathbf{u}}\times\mathbf{B}_0) = \mathbf{B}_0\cdot\overline{\boldsymbol{\omega}}, \tag{2.11}$$

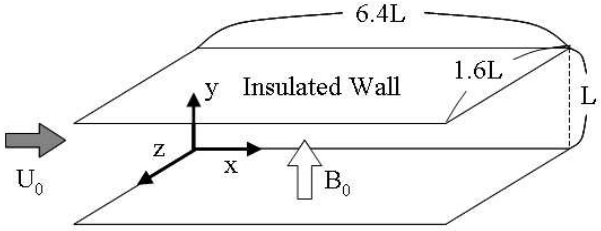

FIGURE 1. Calculation region and coordinate system.

where τ_{ij}^a is the traceless SGS stress tensor and is defined with the SGS stress tensor τ_{ij} by

$$\tau_{ij}^a = \tau_{ij} - \frac{1}{3}\tau_{aa}\delta_{ij}, \quad \tau_{ij} = \overline{u_i u_j} - \overline{u}_i \overline{u}_j. \tag{2.12}$$

2.2. *Computational domain and boundary conditions*

Figure 1 shows the calculation region. In the present study, the directions of x, y, and z, or 1, 2, and 3, are determined as the streamwise, wall-normal, and spanwise directions, respectively. The region size is (L_x, L_y, L_z)=$(6.4L, L, 1.6L)$ with a channel width L. The magnetic field is impressed in the y-direction, and insulator walls are considered.

On the insulator walls, non-slip conditions and non-penetration conditions of the current density are imposed as follows:

$$\mathbf{u} = \mathbf{0}, \quad j_2 = 0 \quad (y = 0, L). \tag{2.13}$$

As a result, the boundary conditions for the GS components are given by

$$\overline{\mathbf{u}} = \mathbf{0}, \quad \frac{\partial \overline{\phi}}{\partial y} = 0 \quad (y = 0, L). \tag{2.14}$$

Periodic boundary conditions are used in the x- and z-directions. In order to specify an MHD flow, one more condition is necessary for the current density in the z-direction. In the present study, one of the objectives is a comparison to the experiment by Brouillette & Lykoudis (1967), which was carried out in a duct with a high aspect ratio. In the present calculation, the net current to sidewalls is assumed zero. That is, an open circuit condition is adopted. The open circuit condition is used to obtain a "two-dimensional" laminar solution in the Hartmann flow. The open circuit condition in the z-direction is

$$\int_0^{L_x} dx \int_0^{L} dy \int_0^{L_z} dz j_3 = 0. \tag{2.15}$$

The above condition for the GS component is given by

$$\int_0^{L} \langle \overline{j}_3 \rangle \, dy = 0, \tag{2.16}$$

where $\langle \quad \rangle$ describes an average in the x-z plane. As a result, $\langle \overline{E}_3 \rangle$ is independent of y:

$$\langle \overline{E}_3 \rangle = -\left\langle \frac{\partial \overline{\phi}}{\partial z} \right\rangle = -B_0 U_0, \tag{2.17}$$

where an average velocity in the channel (a bulk velocity) U_0 is defined by

$$U_0 = \frac{1}{L} \int_0^{L} \langle \overline{u}_1 \rangle \, dy. \tag{2.18}$$

2.3. *Numerical methods*

The above governing equations for the filtered GS component are normalized by the channel width L and the bulk velocity U_0 as follows:

$$\frac{\partial \overline{u}_i}{\partial t} + \overline{u}_j \frac{\partial \overline{u}_i}{\partial x_j} = -\frac{\partial \overline{p}'}{\partial x_i} + \frac{1}{Re}\nabla^2 \overline{u}_i - \frac{\partial \tau^a_{ij}}{\partial x_j} + N\left(-\varepsilon_{ij2}\frac{\partial \overline{\phi}'}{\partial x_j} + \overline{u}_2\delta_{i2} - \overline{u}_i\right) + \left(-\left\langle \frac{\partial \overline{p}}{\partial x}\right\rangle + N\right)\delta_{i1}, \tag{2.19}$$

$$\frac{\partial^2 \overline{\phi}'}{\partial x_k \partial x_k} = \frac{\partial \overline{u}_1}{\partial z} - \frac{\partial \overline{u}_3}{\partial x} = \overline{\omega}_2, \tag{2.20}$$

where Reynolds number Re and interaction parameter N are defined by

$$Re = \frac{U_0 L}{\nu}, \quad N = \frac{\sigma}{\rho}\frac{B_0^2 L}{U_0}, \tag{2.21}$$

so that Hartmann number Ha is defined by

$$Ha = \sqrt{Re\, N} = \sqrt{\frac{\sigma}{\rho\nu}} B_0 L. \tag{2.22}$$

In (2.19) the quantities with a prime ($'$) denote the deviations from the averages in the x-z plane:

$$\overline{p}' = \overline{p} - \langle \overline{p} \rangle, \quad \overline{\phi}' = \overline{\phi} - \langle \overline{\phi} \rangle. \tag{2.23}$$

In the present study, the average pressure gradient $-\langle \partial \overline{p}/\partial x \rangle$ against the streamwise direction is determined such that the total flow rate remains constant:

$$-\frac{\partial \langle \overline{p} \rangle}{\partial x} = -\frac{1}{Re}\left(\left.\frac{\partial \langle \overline{u} \rangle}{\partial y}\right|_{y=1} - \left.\frac{\partial \langle \overline{u} \rangle}{\partial y}\right|_{y=0} \right). \tag{2.24}$$

The normalized continuity equation (2.9), as well as (2.19) and (2.20), is discretized by using both a fully conservative central difference method with fourth-order accuracy in the x- and z-directions, and a second-order accuracy in the y-direction (Morinishi *et al.* 1998). LES is performed with the grid-points $(N_x, N_y, N_z) = (64, 64, 64)$. The time marching scheme is a third-order Adams-Bashforth method, and the coupling between the velocities and the pressure is calculated by the MAC scheme. The Poisson equations for the pressure and the electric potential are solved by the standard FFT method in the x- and z-directions and by the elimination method for tridiagonal matrices in the y-direction. The normalized time step is 1.0×10^{-3}, and each statistic is averaged over 30 non-dimensional time units in the x-z plane after reaching a statistically steady state.

In order to allow comparison with the experiment by Brouillette & Lykoudis (1967), the Reynolds number $Re_D = 58000$, defined by the hydraulic diameter D_h, is changed to $Re = 35000$ defined by the channel width L. That is, if the aspect ratio is $a : b = 5 : 1$, $D_h = 4ab/2(a+b)$ and $L = b$, so that $L/D_h = (a+b)/2a = 0.6$ and $58000 \times 0.6 \approx 35000$. This value corresponds to $Re_\tau = 800 \sim 900$. The examined Ha and $Hr = Ha/Re \times 10^4$ at $Re = 35000$ are shown in Table 1.

2.4. *SGS models*

In the LES, the SGS stress tensor τ^a_{ij} is modeled. The SM, the DSM, and the CSM are examined in the present study.

TABLE 1. Ha and Hr at $Re = 35000$.

Ha	0	22.3	42.4	52.5	58.0	63.0	67.0	71.3	122.2	171.2
$Hr = Ha/Re \times 10^4$	0	6.37	12.1	15.0	16.6	18.0	19.1	20.4	34.9	48.9

In the SM, τ_{ij}^a is modeled with the filter width $\overline{\Delta}$ as

$$\tau_{ij}^a = -2C\overline{\Delta}^2|\overline{S}|\overline{S}_{ij}. \tag{2.25}$$

Here the velocity-strain tensor for GS component $\overline{S}_{ij}$ and its magnitude $|\overline{S}|$ are defined by

$$\overline{S}_{ij} = \frac{1}{2}\left(\frac{\partial \overline{u}_j}{\partial x_i} + \frac{\partial \overline{u}_i}{\partial x_j}\right), \tag{2.26}$$

$$|\overline{S}| = \sqrt{2\overline{S}_{ij}\overline{S}_{ij}}. \tag{2.27}$$

In the SM, $C = C_S^2$ is *a priori* determined, and $C_S = 0.1$ is usually used for channel flows. The wall damping function of the Van Driest type, $1 - \exp(-y^+/25)$, is utilized to express the damping of the turbulent viscosity near walls.

To determine the model parameter in the DSM, the procedure by Germano *et al.* (1991) and Lilly (1992) is used as

$$C = \frac{\langle L_{ij}M_{ij}\rangle}{\langle M_{ij}M_{ij}\rangle}, \tag{2.28}$$

where L_{ij} and M_{ij} are given by

$$L_{ij} = \widehat{\overline{u}_i\overline{u}_j} - \widehat{\overline{u}}_i\widehat{\overline{u}}_j, \tag{2.29}$$

$$M_{ij} = 2\overline{\Delta}^2\widehat{|\overline{S}|\overline{S}}_{ij} - 2\widehat{\overline{\Delta}}^2|\widehat{\overline{S}}|\widehat{\overline{S}}_{ij}. \tag{2.30}$$

In this way, C is dynamically determined in the DSM. To compare the model parameters, $C_S = \sqrt{|C|}$ is used hereafter. The test-filtered velocity $\widehat{\overline{u}_i}$ using a Gaussian filter is calculated for all directions using a Taylor series expansion as

$$\widehat{\overline{f}} = \overline{f} + \frac{\widehat{\Delta}_k^2}{24}\frac{\partial^2 \overline{f}}{\partial x_k^2} + O(\widehat{\Delta}^4), \tag{2.31}$$

where $\widehat{\Delta}$ denotes the test-filter width. It has the following relation with the double filter width $\widehat{\overline{\Delta}}$:

$$\widehat{\overline{\Delta}}^2 = \overline{\Delta}^2 + \widehat{\Delta}^2, \quad \frac{\widehat{\overline{\Delta}}}{\overline{\Delta}} = 2. \tag{2.32}$$

In (2.28), $\langle \quad \rangle$ denotes the averaging of the model parameter in homogeneous directions. The averaging is carried out to avoid any negative values.

In the CSM (Kobayashi 2005), the model parameter is "locally" defined as

$$C = C_{CSM}\,|F_{CS}|^{3/2}\,F_\Omega, \tag{2.33}$$

with

$$C_{CSM} = \frac{1}{22}, \quad F_{CS} = \frac{Q}{E}, \quad F_\Omega = 1 - F_{CS}, \tag{2.34}$$

$$Q = \frac{1}{2}\left(\overline{W}_{ij}\overline{W}_{ij} - \overline{S}_{ij}\overline{S}_{ij}\right) = -\frac{1}{2}\frac{\partial \overline{u}_j}{\partial x_i}\frac{\partial \overline{u}_i}{\partial x_j}, \tag{2.35}$$

$$E = \frac{1}{2}\left(\overline{W}_{ij}\overline{W}_{ij} + \overline{S}_{ij}\overline{S}_{ij}\right) = \frac{1}{2}\left(\frac{\partial \overline{u}_j}{\partial x_i}\right)^2, \tag{2.36}$$

$$\overline{W}_{ij} = \frac{1}{2}\left(\frac{\partial \overline{u}_j}{\partial x_i} - \frac{\partial \overline{u}_i}{\partial x_j}\right), \tag{2.37}$$

where C_{CSM} is a fixed model constant, F_{CS} is the coherent structure function (CSF) defined as the second invariant normalized by the magnitude of a velocity gradient tensor E, F_Ω is the energy-decay suppression function which becomes about 1.1 in homogeneous isotropic turbulences and at the center of turbulent channel flows, and $\overline{W}_{ij}$ is the vorticity tensor in a GS flow field. It is very easy to implement this model in an LES code with the SM because $\overline{S}_{ij}$ and $\overline{S}_{ij}\overline{S}_{ij}$ have been already programmed, and only a sign switch is needed to compute $\overline{W}_{ij}$ and $\overline{W}_{ij}\overline{W}_{ij}$.

3. Results and discussion

Figure 2 shows the skin friction coefficient C_f as a function of $Hr = Ha/Re \times 10^4$. The experimental data at $Re_D = 58000$ for 5:1 aspect ratio (Brouillette & Lykoudis 1967) and $Re_D = 53000$ for 5.8:1 aspect ratio (Reed & Lykoudis 1978) are shown in the figure. The Reynolds number $Re_D = 53000$ in a duct corresponds to $Re = 31000$ in the present plane channel. In the figure, the dashed line indicates the two dimensional laminar solution $C_f = 2Ha/Re$ (i.e., $C_f \times 10^3 = Hr/5$). For the experiment in 1967, as Hr increases from $Hr = 0$, C_f slightly decreases and has a minima around $Hr = 12$. Then, C_f increases to a local maximum (the "hump") at around $Hr = 23$ and subsequently decreases to a local minimum (the "dip") at around $Hr = 30$. For the experiment in 1978, C_f increases and reaches a local maximum (the "hump") at around $Hr = 18$ before its subsequent decline to a minimum (the "dip") at around $Hr = 24$. For higher Hr values, both C_f curves approach the laminar line.

In the computational result with SM, as Hr increases from zero, C_f decreases, and a "final damp" takes place at $Hr = 12.1$. The final damp refers to the state in which the near-wall velocity fluctuation that is not only perpendicular to the magnetic field but also parallel to it has been completely damped, and the dip is observed. The state was clearly observed in the experiment of MHD pipe flows (Gardner & Lykoudis 1971). For higher Hr, C_f keeps a higher value than the laminar line. This occurs because the model parameter in the SM is kept constant in a high magnetic field, and the turbulent eddy viscosity is non-zero as long as $\overline{S}_{ij}$ has a value. This defect in the SM was pointed out by Shimomura (1991), who improved the model by explicitly imposing the effect of the magnetic field on the model parameter. In the DSM result, as Hr increases from zero, C_f decreases and the final damp takes place at $Hr = 16.6$. With CSM, C_f increases slightly and then decreases from $Hr = 12.1$. The final damp takes place at $Hr = 18.0$.

The difference between the final damp of the CSM and that of the DSM is due to the determination of the model parameter. The model parameter of the CSM is locally determined, and the fluctuations are reflected in the shear stress. On the other hand, the

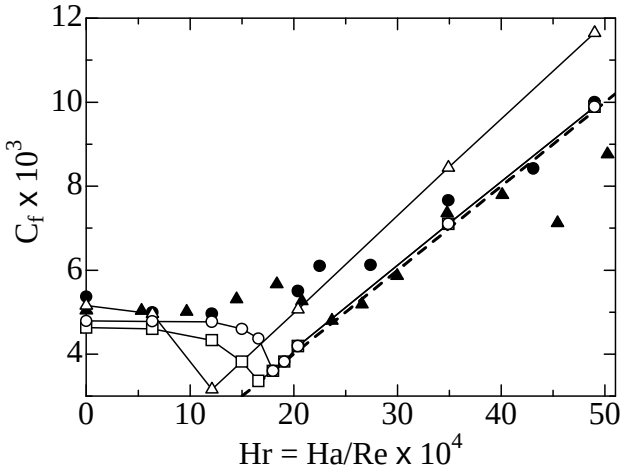

FIGURE 2. Skin friction coefficient C_f computed with three SGS models (–○–, CSM; –□–, DSM; –△–, SM) as a function of $Hr = Ha/Re \times 10^4$ at $Re = 35000$: •, the experimental data of Brouillette & Lykoudis (1967) for $Re_D = 58000$; ▲, the experimental data of Reed & Lykoudis (1978) for $Re_D = 53000$; - - - - , the laminar value of the two dimensional solution $C_f = 2Ha/Re$ (i.e., $C_f \times 10^3 = Hr/5$).

model parameter of the DSM is averaged in the homogeneous directions so that the shear stress is underestimated. The difference is represented by $\langle C|\overline{S}|\overline{S}_{ij}\rangle - \langle C\rangle\langle|\overline{S}|\overline{S}_{ij}\rangle$. In turbulence without the magnetic field, even though C is averaged, the local $|\overline{S}|\overline{S}_{ij}$ value fluctuates significantly. As a result, the difference between $\langle C|\overline{S}|\overline{S}_{ij}\rangle$ and $\langle C\rangle\langle|\overline{S}|\overline{S}_{ij}\rangle$ is small. In the magnetic field, however, the fluctuation of $|\overline{S}|\overline{S}_{ij}$ is suppressed so that the effect of the local fluctuation of C on τ_{ij} is revealed. The present result of the DSM may be improved by using the localization models proposed by Ghosal *et al.* (1995) and by Piomelli *et al.* (1995). Figure 3 shows the profiles of (a) the Reynolds shear stress and (b) the mean streamwise velocity computed with CSM and DSM at $Hr = 15.0$. The shear stress from DSM is smaller than that from CSM. Consequently, DSM predicts the laminarization more rapidly than CSM. The mean streamwise velocity from DSM shows a usual laminarized flow in comparison with that from CSM. In the range $12.1 < Hr \leq 16.6$, the reduction of C_f that is owing to the decrease in the shear stress dominates the rise of C_f that is owing to the effect of the Hartmann flattening.

For high $Hr(\geq 20.4)$, the CSM and the DSM reproduce the laminarization well, although the LES with CSM and DSM does not reproduce the distinct hump. Figure 4 shows the profiles of (a) model parameter C_S, (b) model parameter $C\overline{\Delta}^2$ near a wall for CSM, DSM, and SM, and (c) $C\overline{\Delta}^2$ for the DSM, all at $Hr = 48.9$. For the CSM and the DSM, the model parameter is drawn as $C_S = \sqrt{|C|}$ in Figs. 4(a) and (b). In Fig. 4(a), while C_S for SM at $Hr = 48.9$ is the same as that at $Hr = 0$, C_S of the DSM automatically decreases as Hr increases, so that the laminarization is reproduced. Although C_S of the CSM becomes higher than that of the SM, the CSM reproduces the laminarization as well as does the DSM. This is due to the existence of coherent structures and to the slight shear stress in the laminarized MHD flow. In a previous paper, it was confirmed that the model parameter for CSM approaches zero in a laminar flow (Kobayashi 2005). Thus, the model parameter profile for CSM indicates that the laminarized MHD flow is different from the usual laminar flow without a magnetic field.

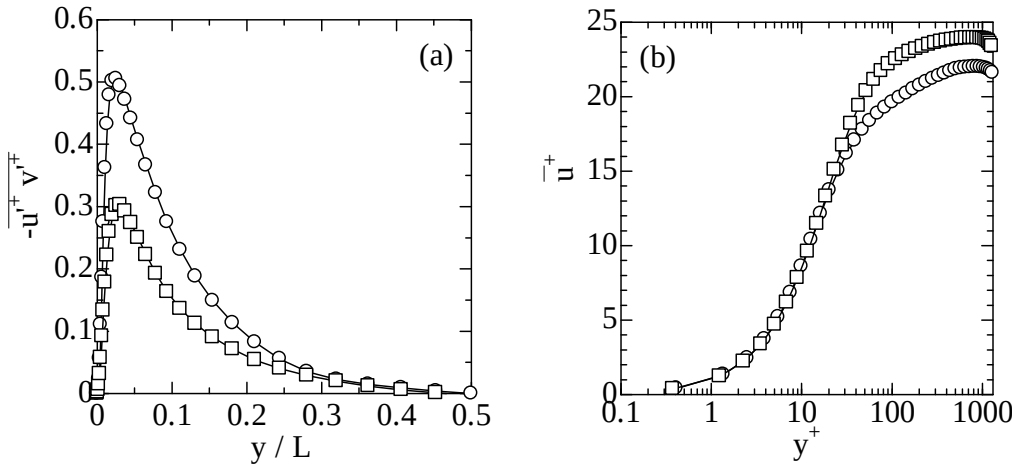

FIGURE 3. Profiles of (a) Reynolds shear stress and (b) mean streamwise velocity computed with CSM and DSM at $Hr = 15.0$: –○–, CSM; –□–, DSM.

The CSM can reproduce the laminarization due to the lack of shear stress in the core region of the laminarized MHD flow. In the present flow, C_S in the core flow does not affect the turbulent eddy viscosity as seen in (2.25), because $|\overline{S}| \approx 0$. As shown in Fig. 4(b), the existence of the turbulent eddy viscosity in the SM is caused by $C\overline{\Delta}^2$ near the walls. The model parameters of the CSM and the DSM near the wall are smaller than that of the SM. As a result, in the Hartmann layer near a wall with a strong shear stress, the turbulent eddy viscosities for the CSM and DSM become small. Note that the profile of $C\overline{\Delta}^2$ for DSM in Fig. 4(b) disappears in the core flow. From Figs. 4(a) and (c), it is found that the large negative value appears in spite of the averaging of the model parameter in the homogeneous directions. Fortunately, since $|\overline{S}| \approx 0$, the turbulent eddy viscosity is negligible in comparison with the molecular viscosity, so the negative value does not cause a numerical instability. In this case, it is impossible to find out the true profile of C using the DNS, because $\tau_{ij} \approx 0$ and $|\overline{S}| \approx 0$ in (2.25) so that C is an arbitrary constant.

Figure 5 shows the CS at (a) $Hr = 0$ and at (b) $Hr = 48.9$ extracted by $F_{CS} = 0.4$. The walls exist above and below in the figures, the magnetic field is impressed perpendicular to the walls, and the fluid flows from left to right. Although the mesh size in the normal direction becomes small near the wall, the figure is drawn as though there is equal space and the CS near walls is enlarged. The CS with the large F_{CS} exists around the center of the channel flow at $Hr = 0$, as shown in Fig.5(a), although the CS extracted by the second invariant Q exists near walls (Kobayashi 2005). On the other hand, at $Hr = 48.9$ as shown in Fig.5(b), the CS extracted by F_{CS} becomes large and aligns along the magnetic field. The CS extracted by Q shows similar behavior, as was pointed out in an isotropic turbulence by Miyauchi & Tanahashi (2001) and in a channel by Lee & Choi (2001). This result shows a transient CS, the CS would disappear after sufficiently long time. Thus, the laminarization of turbulent MHD channel flows with the magnetic field differs from the usual laminar flows without the magnetic field.

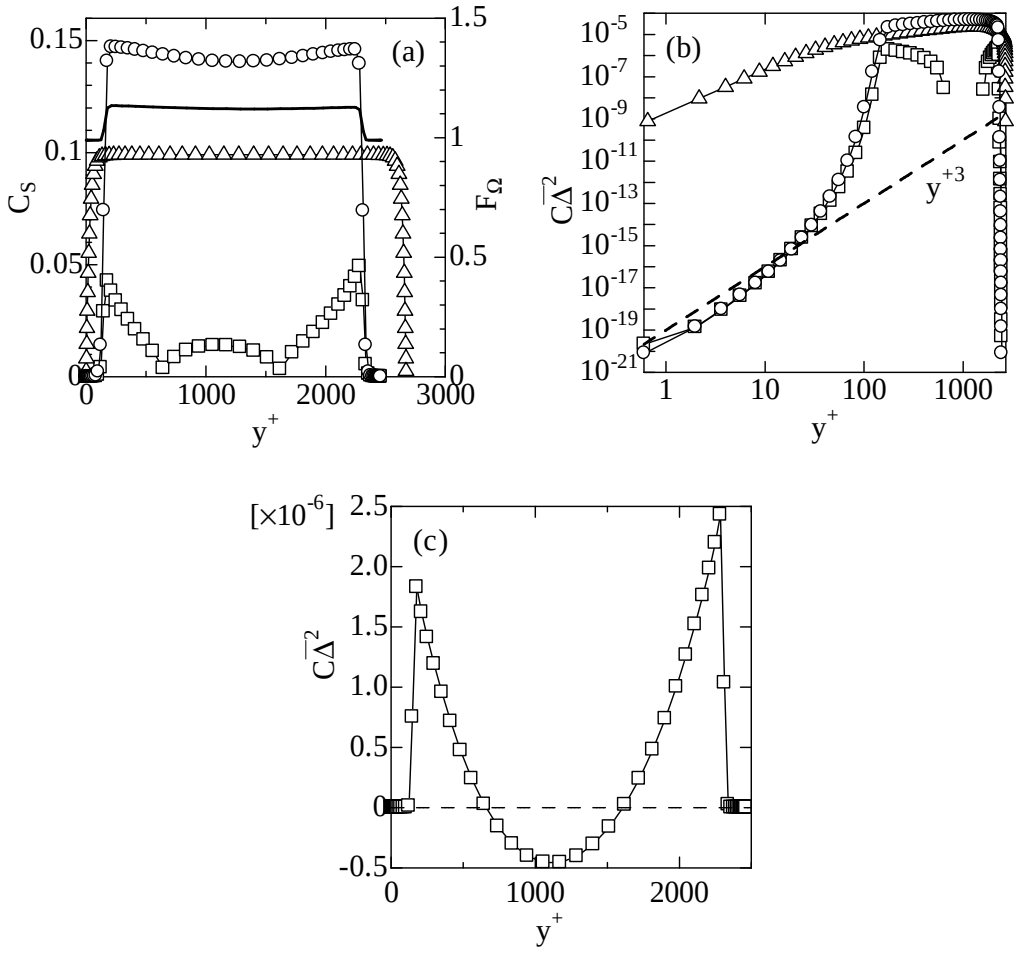

FIGURE 4. Profiles of (a) model parameter C_S (——, F_Ω), (b) model parameter $C\overline{\Delta}^2$ near a wall for CSM, DSM, and SM, and (c) model parameter $C\overline{\Delta}^2$ for DSM, at $Hr = 48.9$: –○–, CSM; –□–, DSM; –△–, SM.

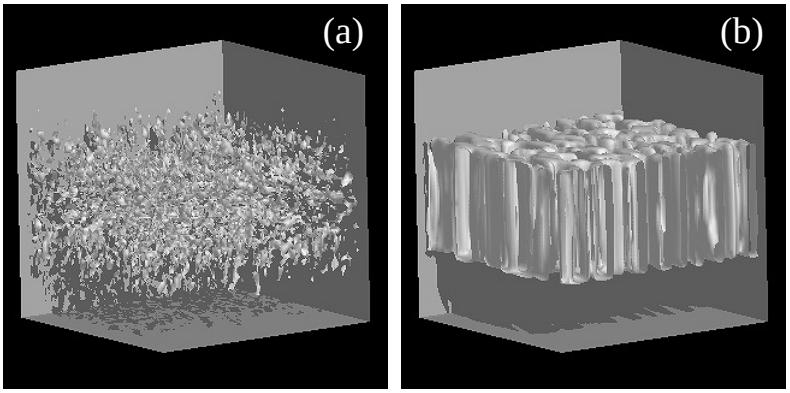

FIGURE 5. Coherent structures at (a) $Hr = 0$ and at (b) $Hr = 48.9$ extracted by $F_{CS} = 0.4$.

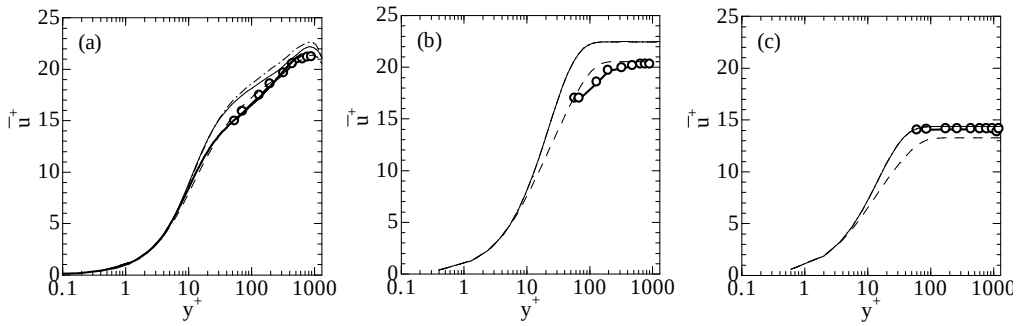

FIGURE 6. Mean streamwise velocity profiles for (a) $Hr = 0$, (b) $Hr = 20.4$, and (c) $Hr = 48.9$: ——— , CSM; — — — , DSM; - - - - , SM; –○–, experiment; ━━━ , DNS $Re_\tau = 590$.

Figure 6 shows the mean streamwise velocity profiles for (a) $Hr = 0$, (b) $Hr = 20.4$, and (c) $Hr = 48.9$, which arise from a detailed investigation of the turbulent MHD channel flow. In Fig. 6, the experimental data (Brouillette & Lykoudis 1967) are drawn, and in Fig. 6(a) the DNS result at $Re_\tau = 590$ (Moser *et al.* 1999) is added for reference. Figure 6(a) shows that for $Hr = 0$, the profiles from the DNS and SM agree closely with the experimental data, whereas the CSM and DSM slightly overestimate the profile. In Fig. 6(b) for $Hr = 20.4$, the mean streamwise velocity at the center of the SM is close to that of the experiment, but those from CSM and DSM coincide and show an overestimation in comparison with the experiment. As seen in Fig. 2, the experiment shows the hump, but the CSM and DSM profiles have already reproduced the laminarization. The agreement between the SM and the experiment in Fig. 6(b) is coincidental because, as shown later in Fig. 7, it is caused by the indelible Reynolds shear stress near the wall in SM. In Fig. 6(c) for $Hr = 49.0$, the CSM and DSM agree with the experiment and they closely reproduce the laminarization. The SM, however, underestimates the profile in comparison with the experiment, because the turbulent eddy viscosity of the SM remains in the magnetic field. Since the CSM gives almost identical results as the DSM, the results of the DSM are not shown hereafter.

Figure 7 shows the Reynolds shear stress profiles for Hr =6.37, 12.1, and 20.4. At Hr =6.37, the CSM and SM maintain a strong shear stress, so that the predictions of C_f are close to the experiment as shown in Fig. 2. At Hr =12.1, while the CSM keeps a strong shear stress, the SM loses the shear stress except near the wall. This is why the laminarization arises in Fig. 2. At Hr =20.4, the shear stress of the CSM disappears in a whole region, but that of the SM remains near the wall. As a result, the coincidence of C_f occurs in Fig. 6(b).

Figure 8 shows the profiles of the rms of velocity fluctuations (a) $\overline{u}_{rms}$, (b) $\overline{v}_{rms}$, and (c) $\overline{w}_{rms}$ for Hr =6.37, 12.1, and 20.4. At Hr =6.37, the performance of the CSM is similar to that of the SM. At Hr =12.1, all fluctuations from SM drastically disappear, while the CSM keeps strong velocity fluctuations in all components. Shimomura (1991) has already pointed out this defect of the SM with his model. At Hr =20.4, the shear stress of the CSM disappears as shown in Fig. 7, but the velocity fluctuations remain due to the diffusion terms in turbulent kinetic energy equations. This feature is reported in the experiment by Reed & Lykoudis (1978) and in the DNS study by Lee & Choi (2001); the Reynolds shear stress is rapidly suppressed by the magnetic field, but the velocity fluctuations remain.

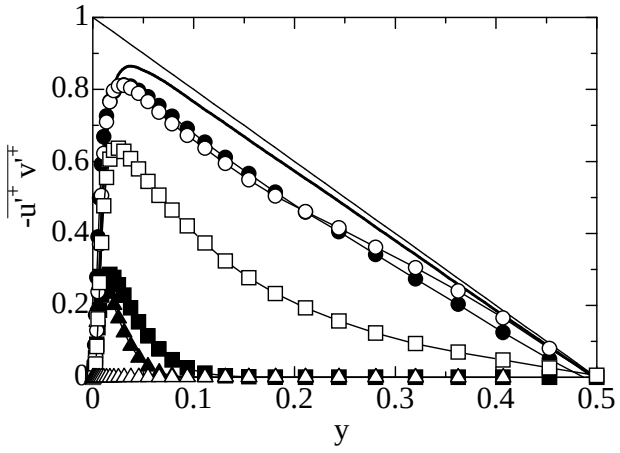

FIGURE 7. Reynolds shear stress profiles for Hr =6.37 (–○–, CSM; –●–, SM), 12.1 (–□–, CSM; –■–, SM), and 20.4 (–△–, CSM; –▲–, SM) : ——, DNS $Re_\tau = 590$.

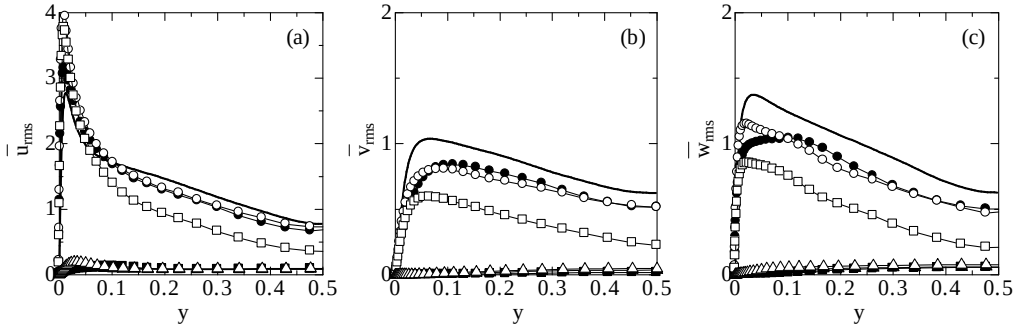

FIGURE 8. Profiles of the rms of velocity fluctuations: (a) $\overline{u}_{rms}$, (b) $\overline{v}_{rms}$, and (c) $\overline{w}_{rms}$ for Hr =6.37 (–○–, CSM; –●–, SM), 12.1 (–□–, CSM; –■–, SM), and 20.4 (–△–, CSM; –▲–, SM) : ——, DNS $Re_\tau = 590$.

4. Conclusions

At low magnetic Reynolds number, the laminarization in turbulent MHD channel flows by a magnetic field perpendicular to insulated walls has been examined using the CSM, the DSM, and the SM. The Hartmann number at which the laminarization takes place becomes higher with CSM or DSM than it does with SM, as the shear stress predicted by SM in the core flow rapidly disappears.

The CSM predicts a higher Hartmann number at which the transition to the laminarized MHD flow takes place than does the DSM, because the model parameter in CSM is locally determined and the fluctuations are reflected in the shear stress. On the other hand, the model parameter in DSM is averaged in the homogeneous directions, so the shear stress is somewhat underestimated in the transitional Hartmann number.

In the laminarized MHD flow, the SM gives the indelible Reynolds shear stress near the wall, because the model constant near the wall remains large. On the other hand, the near-wall model parameters of CSM and DSM drastically decrease, and Reynolds shear stress rapidly decreases in the whole region, but small velocity fluctuations remain owing to the diffusion terms in turbulent kinetic energy equations. As a result, the CSM and DSM can reproduce the laminarization of turbulent MHD channel flows in the experiments

(Brouillette & Lykoudis 1967; Reed & Lykoudis 1978), although they were not able to reproduce the distinct "hump" in the profile of C_f. The subsequent "dip" is located at lower Hr than in the experiment. This may be due to the inadequacies of the SGS models or to the side-wall effect. For the former, explicit imposition of the effect of the magnetic field on the model parameters may be needed. For the latter, simulations of turbulent MHD duct flows are needed.

In the laminarized MHD flow, the behavior of the model parameters of the CSM and the DSM is different at the center of the channel. Whereas the model parameter of the DSM becomes negative, that of the CSM approaches a positive value larger than that of the SM. The behavior of the CSM indicates the existence of CS in the laminarized MHD flow. This is different from the disappearance of the model parameter in a usual laminar flow without a magnetic field. The CS becomes large and aligns itself along the magnetic field. However, the mean streamwise velocity gradient approaches zero in the core flow due to the Hartmann effect, and consequently the model parameter does not affect the turbulent eddy viscosity.

In the future, LES of the turbulent MHD flows in a duct and a pipe is needed to reveal the effect of sidewalls and to make quantitative comparisons with the experiments.

Acknowledgments

The author would like to thank Professor Y. Shimomura for suggesting an examination of the SGS models in turbulent MHD channel flows, Professor Emeritus A. Yoshizawa, Professor P. Moin, Professor Y. Shimomura, Professor K. Ueno, Dr. M. Wang, and Dr. M. Herrmann for valuable discussion and comments, and Dr. M. Wang and Dr. M. Herrmann for improving the presentation of this manuscript. The author is deeply grateful to Professor P. Moin for providing the research opportunity as a senior visiting fellow at the Center for Turbulence Research.

REFERENCES

Brouillette, E. C. & Lykoudis, P. S. 1967 Magneto fluid mechanic channel flow. I. Experiment. *Phys. Fluids.* **10**, 995–1001.

Gardner, R. A. & Lykoudis, P. S. 1971 Magneto fluid mechanic pipe flow in a transverse magnetic field. Part 1. Isothermal flow. *J. Fluid Mech.* **47**, 737–764.

Germano, M., Piomelli, U., Moin, P., & Cabot, W. H. 1991 A dynamic subgrid-scale eddy viscosity model. *Phys. Fluids A* **3**, 1760–1765.

Ghosal, S., Lund, T. S., Moin, P. & Akselvoll, K. 1995 A dynamic localization model for large-eddy simulation of turbulent flows. *J. Fluid Mech.* **286**, 229–255.

Knaepen, B. & Moin, P. 2004 Large-eddy simulation of conductive flows at low magnetic Reynolds number. *Phys. Fluids.* **16**, 1255–1261.

Kobayashi, H. 2005 The subgrid-scale models based on coherent structures for rotating homogeneous turbulence and turbulent channel flow. *Phys. Fluids* **17**, 045104.

Lee, D. & Choi, H. 2001 Magnetohydrodynamic turbulent flow in a channel at low magnetic Reynolds number. *J. Fluid Mech.* **439**, 367–394.

Lilly, D. K. 1992 A proposed modification of the germano subgrid-scale closure method. *Phys. Fluids A* **4**, 633–635.

Miyauchi, T. & Tanahashi, M. 2001 Coherent fine scale structure in turbulence. *IUTAM Symposium on Geometry and Statistics of Turbulence*, (Kluwer, Netherlands), 67–76.

Morinishi, Y., Lund, T. S., Vasilyev, O. V., & Moin, P. 1998 Fully conservative higher order finite difference schemes for incompressible flow. *J. Comp. Phys.* **143**, 90–124.

Moser, R. D., Kim, J. & Mansour, N. N. 1999 Direct numerical simulation of turbulent channel flow up to $Re_\tau = 590$. *Phys. Fluids* **11**, 943–945.

Piomelli, U. & Liu, J. 1995 Large-eddy simulation of rotating channel flows using a localized dynamic model. *Phys. Fluids* **7**, 839–848.

Reed, C. B. & Lykoudis, P. S. 1978 The effect of a transverse magnetic field on shear turbulence. *J. Fluid Mech.* **89**, 147–171.

Schumann, U. 1976 Numerical simulation of the transition from three- to two-dimensional turbulence under a uniform magnetic field. *J. Fluid Mech.* **74**, 31–58.

Shimomura, Y. 1991 Large eddy simulation of magnetohydrodynamic turbulent channel flows under a uniform magnetic field. *Phys. Fluids A* **3**, 3098–3106.

Smagorinsky, J. 1963 General circulation experiments with the primitive equations. I. The basic experiment. *Mon. Weather Rev.* **91**, 99–152.